Dynamic analysis and design of impact attenuator structures for a Formula Student prototype

André Miguel Almeida Santos
andre.m.santos@tecnico.ulisboa.pt
Instituto Superior Técnico, Universidade de Lisboa, Portugal
June, 2017

Abstract

The current energy-absorbing structure solution is analysed and a numerical model is developed. Preliminary tests with aluminium and carbon fibre tubes follow, where the energy absorbing process is better understood and an important numerical parameter (Crush Stress) is fine-tuned. A set of quasi-static tests that are able to predict the Crush Stress of different lay-ups is developed and used subsequently.

Several solutions are explored through a series of new numerical models and optimization processes, which are only possible after several time-reducing techniques and algorithms are applied. The different obtained options are later weighted, selected, manufactured and tested after which the experimental results are presented and explained. A final lighter solution is once again presented, manufactured and successfully tested.

I. Introduction

During the last few decades, there has been an overall increase in the use of composite materials in several industries, due to the decrease of cost while allowing for lighter, yet more complex, designs. In the automotive industry, safety is a major concern which has increased the weight of cars and, as a consequence, the fuel consumption. Replacing aluminium or steel Impact Attenuators (IA) with composites can reduce the weight while maintaining, or even increasing, the occupants safety, due to higher Specific Energy Absorption (SEA), Jones and Wierzbicki [1], a.G Mamalis et al. [2].

In the Formula Student competition, students are challenged to design, build and test a race car according to a specific set of rules by Formula Society of Automotive Engineers (FSAE), FSAE [3]. Obradovic et al. [4] successfully simulated and tested carbon fibre tubes and a composite impact attenuator for the University of Torino's Formula Student team. Boria and Belingardi [5] also analysed the crush behaviour of carbon fibre tubes. Hussein et al. [6] studied the crush behaviour of empty and honeycomb-filled squared carbon fibre tubes, concluding that the latter absorb more energy but lose weight efficiency. Similar but more complex analysis have been performed in Formula 1 cars, where Heimbs and Strobl [7] performed a crash analysis on the front impact structure using LS-DYNA [8].

Browne [9] presented a series of experimental tests and analytical calculations in order to design a structural nose capable of absorbing the required energy.

i. Optimization

In this paper multiple multi-objective nonlinear programming problem are defined: Custódio et al. [10], Franco Correia et al. [11] or Miettinem [12].

Find n design variables $\boldsymbol{x} = (x_1, x_2, ..., x_n) \in \Omega \subseteq \mathbb{R}^n$ which minimize (2).

$$min \quad F(\boldsymbol{x}) \equiv (f_1(\boldsymbol{x}), f_2(\boldsymbol{x}), ..., f_m(\boldsymbol{x})) \quad (1)$$
$$s.t. \quad \boldsymbol{x} \in \Omega \quad (2)$$

Involving $m > 1$ objective functions or objective function components $f_j : \Omega \subseteq \mathbb{R}^n \rightarrow \mathbb{R} \cup \{+\infty\}, j = 1, ...m$ and being Ω a feasible region.

Furthermore, it is assumed that all the objective functions to be of the black-box type, meaning that only function values are available and can be used to solve the problem. This is a common feature in many situations in which computation of the problem functions is the result of time-consuming and complex simulation programs.

DMS Custódio et al. [10] is a derivative-free method for multiobjective optimization problems, which does not aggregate any components of the objective function. It is inspired by the search/poll paradigm of direct-search methods of directional type, extended from single to multiobjective optimization and uses the concept of Pareto dominance to maintain a list of feasible non-dominated points.

In the DMS method, the constraints are handled using an extreme barrier function. Details are omitted in the present paper and the reader is referred to Custódio et al. [10] for a more complete description of this method.

II. IA Preliminary Simulations and Testing

i. Aluminium Tubes

i.1 Experimental Analysis

An aluminium tube was chosen as a first concept for a self-developed IA. A circular cross-section was chosen, due to its axisymmetry, with 90 millimetres of diameter, 300 millimetres of length and two millimetres of thickness.

An high speed camera was used to record the event and an example of the resulting frames may be observed in figure 1 where a concertina mode of failure was obtained. While the first tube folded eight full times, the second only folded seven times and began the eighth.

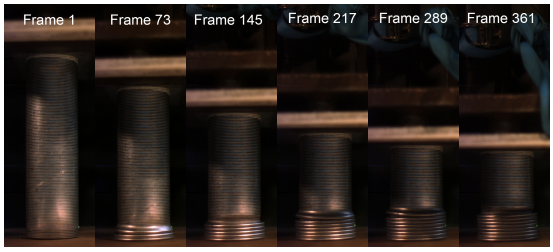

Figure 1: *High-speed frames from the first test.*

A tracking algorithm was implemented in order to retrieve the displacement versus time plot of the steel mass during the impact (figure 3).

The difference observed on the maximum displacement between the first and second tests was probably due to a small difference on the initial velocity.

The raw data presents a chaotic evolution with acceleration peaks above $1600 m/s^2$. A low-pass filter followed by an high-pass filter (with a cut-off frequency of 100Hz and 0.75Hz, repectively) had to be employed in order to eliminate undesired frequencies. In figure 2, an average between the two accelerometers was performed for the first and second test.

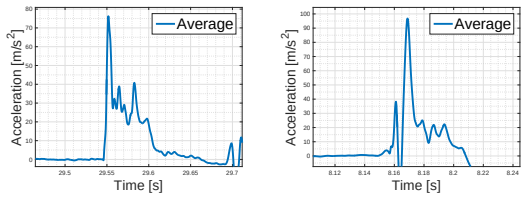

(a) Accelerometers average. (b) Accelerometers average.

Figure 2: *Post-processing of the accelerometer data from the first and second tests.*

i.2 Numerical Model

After the experimental tests with the aluminium tubes, a numerical model was developed.

The tube was modelled in Abaqus [13] with shell elements, where the supporting plate and the impacting plate were also modelled using rigid elements. A mass of 300 kg was associated with the impacting plate. A general contact (with self-contact) rule was used between the tube and the impacting plate, and between the tube and the supporting plate. An encastre boundary condition was imposed on the supporting plate and the impacting plate had its transversal directions and rotations locked. An initial condition of $7m/s$ was also imposed on the impacting plate.

A maximum error of 3.5% was obtained between the first test and the numerical model prediction. As for the second test, a maximum error of 5.5% was achieved (figure 3). In figure 4 an overview of the final deformation shape results is provided.

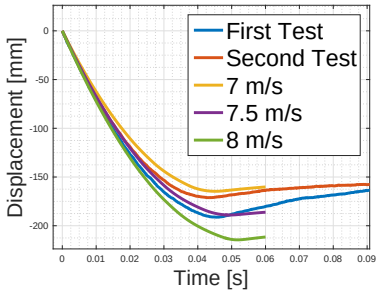

Figure 3: *Initial velocity variation.*

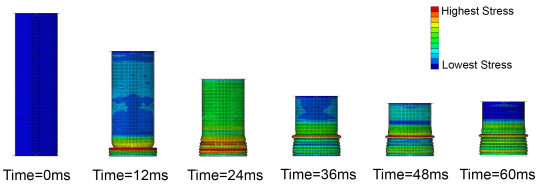

Figure 4: *Final results from the aluminium tubes simulation.*

ii. Carbon Fibre tubes

ii.1 Experimental Analysis

The next step was to change to an orthotropic material such as carbon fibre, while maintaining the geometry. The material used was pre-impregnated, uni-directional tape, carbon fibre.

The lay-up was defined as $[(0°/90°)_2]_s$.

A very similar setup to the aluminium tubes was used. Three carbon fibre tubes were tested. However, the first test was considered invalid due to a setup problem.

The high-speed frames retrieved from the second test are presented in figure 5.

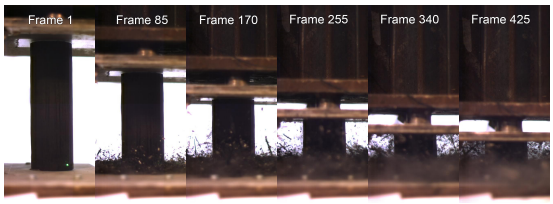

Figure 5: *Frames recorded by the high speed camera during the carbon fibre tube's second test.*

Using the open-source program Tracker [14], the vertical position of the weight was tracked on both tests.

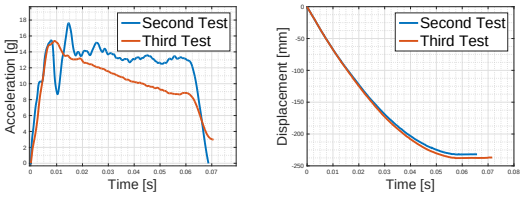

(a) Acceleration plots, high-pass filter with average and impact peak comparison..

(b) Displacement versus time plot computed from the high speed camera data for the carbon fibre tubes.

Figure 6: *Acceleration and displacement plots.*

By comparing the displacement curves obtained through the high-speed camera a maximum difference of 2.4% was achieved between them (figure 6).

A third order low-pass Butterworth filter with a cut-off frequency of 100 Hz was used.

By averaging the three curves, the acceleration curve at the CG was obtained for both tests (figure 6(a)).

ii.2 Numerical Model

A commercial finite-element software - Abaqus [13] Explicit with the CZone [15] algorithm - was used in order to simulate the full impact. This algorithm uses a constant property called Crush Stress which is, by definition, the stress required to maintain a stable crush front.

An isotropic Crush Stress was considered and it was iterated until a good fit to the experimental data was achieved.

A contact pair was established between the barrier and the AIP.

While the second test was found to have a fitted Crush Stress of 68MPa, the third test was fitted with a Crush Stress of 66MPa, with about 4% and 2% error, respectively (figure 7(b)). The simulation was able provide an approximation for the displacement curve of both tests with an error under 5%.

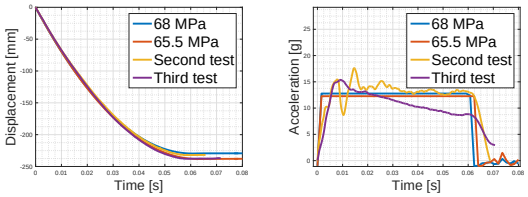

(a) Comparison between the fitted simulation and the experimental displacement results.

(b) Comparison between the fitted simulation and the experimental acceleration results.

Figure 7: *Numerical model and experimental comparison.*

On figure 8, the frame results from the simulation are presented.

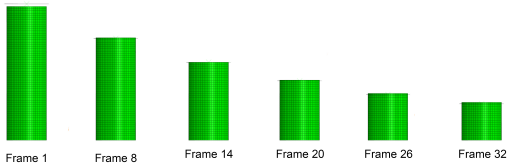

Figure 8: *Frame results from the Abaqus [13] simulation.*

ii.3 Crush Stress Validation

It is not feasible to continually test full scale components in order to achieve a crash-worthy lay-up design so a different method to compute the Crush Stress is needed.

A carbon fibre plate with a similar lay-up to the one used on the tubes was manufactured and several test pieces were cut (figure 9(a)).

The specimen were crushed with the setup shown in figure 9(b).

(a) Test specimens cut at 0° with small indentations on the top.

(b) Setup used for specimen crushing.

Figure 9: *Crush stress setup and specimens..*

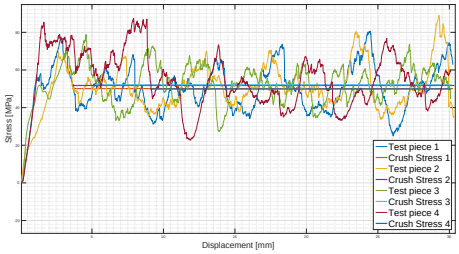

Figure 10: *Stress versus displacement plot results.*

The stress versus displacement plots are presented in figure 10, the average of the four tests is the Crush Stress value.

The mean Crush Stress of the four specimens is 51MPa with a maximum variation of 2%.

The value obtained using the test specimens is 23.6% lower than the one obtained through simulation fitting.

Mamalis et al. [16] showed that the SEA increased during dynamic loads, when compared to static loads, which may explain the lower Crush Stress obtained.

III. IA Simulations and Optimization

i. Crush Stress Prediction

A set of similar tests to the previous section was performed on the carbon fibre available to use in the impact attenuator was planned and executed in order to obtain an orthotropic Crush Stress, so the specimens were cut with different inclinations in intervals of 15°.

A different carbon fibre than the one used in section ii was supplied by the team. The new material differs from the previous as it is bi-directional prepreg, twill woven, high strength, carbon fibre.

For each orientation an average value was assumed. In figure 11, a representation of the Crush Stress in each direction is presented, where the distance to the origin is the Crush Stress value for that particular direction and where the angle is between the direction of impact and the fibre direction.

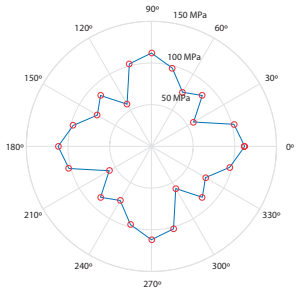

Figure 11: *Crush Stress results summary.*

ii. Structural Nose

ii.1 Numerical Model

The main advantage of a structural nose is that it replaces the IA. Abaqus Explicit with the CZone [15] algorithm was used.

In figure 12, one can see an example of the frame results from the nose simulation.

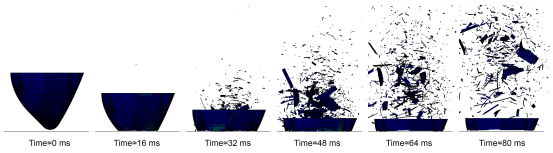

Figure 12: *Structural nose frame results.*

ii.2 Coreless optimization

Efforts were made in order to reduce the time of each simulation to a feasible value.

Besides the symmetry condition imposed, which reduced the time by 70% (section ii.1), a 10 mm mesh was used, which reduced the time by 60%, the optimization was run on a much powerful i7 Intel processor, which reduced the time by 33% and, finally, an algorithm was created in order to reduce the need to run the entire impact time, which, in average, reduced the time by 50%.

A MOO problem consists in finding the non-dominated solutions that minimize, simultaneously, the mass of the nose (f_1) and the maximum acceleration (f_2) obtained throughout the impact (3a). The main objective in this optimization will be to reduce the weight. The minimization of the maximum acceleration will serve as a performance criteria, as a lower acceleration will result in a higher safety coefficient.

$$\min_{\boldsymbol{x}\in\Omega} \quad F(\boldsymbol{x}) \equiv (f_1(\boldsymbol{x}), f_2(\boldsymbol{x})) \tag{3a}$$

$$\begin{aligned} s.t. \quad & x_i \in \{4,5,...,10\} \quad i = 1,...,7 \\ & x_i \in \{1024,1025,...,2047\} \quad i = 8,...,14 \end{aligned} \tag{3b}$$

$$\begin{aligned} max(A(\boldsymbol{x})) &\leqslant 35g \\ mean(A(\boldsymbol{x})) &\leqslant 20g \end{aligned} \tag{3c}$$

A symmetrical lay-up assumption was made. The number of layers of each different zone is imposed by 3b.

The remaining seven discrete variables, $x_8, ..., x_{14}$ represent the orientation of each set of layers previously determined by $x_1, ..., x_7$, respectively.

In figure 13 all the points that complied with the constraints are represented. A viable solution would probably be solution 4, since it is only 3% heavier but has a maximum acceleration 50% lower than solution 1 and 5.

None of these solutions is lighter than the aluminium honeycomb option.

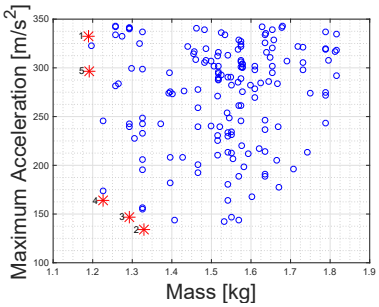

Figure 13: *The nondominated solutions obtained from the optimization of a coreless structural nose is represented by the red stars.*

ii.3 Core Optimization

In order to add stiffness, while maintaining a low weight, a core material is included.

An optimization problem was defined and solutions analysed. The objective functions, f_1 and f_2, and the acceleration constraints remain the same (4a and 4c). There are six variables representing the number of layers and six variables representing the orientations of each layer, ranging from 128 to 255.

$$\min_{\boldsymbol{x}\in\Omega} \quad F(\boldsymbol{x}) \equiv (f_1(\boldsymbol{x}), f_2(\boldsymbol{x})) \tag{4a}$$

$$\begin{aligned} s.t. \quad & x_i \in \{1,2,...,7\} \quad i = 1,...,6 \\ & x_i \in \{128,129,...,255\} \quad i = 7,...,12 \\ & x_i \in \{0,1,...,63\} \quad i = 13 \end{aligned} \tag{4b}$$

$$\begin{aligned} & max(A(\boldsymbol{x})) \leqslant 35g \\ & mean(A(\boldsymbol{x})) \leqslant 20g \end{aligned} \tag{4c}$$

There's also a new variable to account for the possibility of a core.

In figure 14, all points, that complied with the constraints, are represented. The lightest, nondominated, solution presented a mass of 392.5g, with a maximum acceleration of 168.4m/s^2.

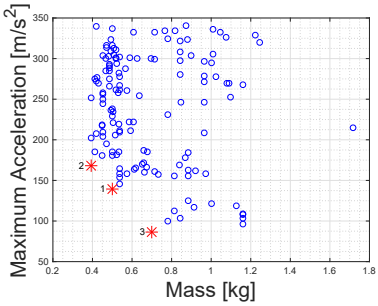

Figure 14: *The red stars represent the nondominated solutions obtained from the optimization of the structural nose, with core.*

iii. Crashbox

iii.1 Numerical Model

By the FSAE rules the crashbox geometry is completely free to take any shape it can, bounded by packaging and minimum limits. Thus, geometrical variables were added.

The geometry was assumed to be an offset of the minimum dimension and internal vertical and horizontal cross-section divisions were also allowed.

iii.2 Optimization

The objective functions, as well as the acceleration constraints, remain the same (5a and 5c) as in previous sections. However, the number of variables increased to 16 in order to account for the geometry (bounded as in 5b).

Variables x_1, x_2 and x_3 represent the length, width and height of the crashbox (in millimetres). The variables x_4 and x_5 represent the number of internal cross-section divisions. The internal division possibilities, figure 15(a) presents a schematic of all possible combinations.

$$\min_{\boldsymbol{x}\in\Omega} \quad F(\boldsymbol{x}) \equiv (f_1(\boldsymbol{x}), f_2(\boldsymbol{x})) \tag{5a}$$

$$
\begin{aligned}
s.t. \quad & x_1 \in \{200, 205, ..., 400\} \\
& x_2 \in \{100, 105, ..., 300\} \\
& x_3 \in \{200, 205, ..., 400\} \\
& x_4 \in \{1, 2, ..., 5\} \\
& x_5 \in \{1, 2\} \\
& x_i \in \{1, 2, ..., 7\} \quad i = 6, ..., 9 \\
& x_j \in \{128, 129, ..., 255\} \quad j = 10, ..., 13 \\
& x_{14} \in \{1, 2, 3, 4\} \\
& x_k \in \{1, 2\} \quad k = 15, 16
\end{aligned} \tag{5b}
$$

$$
\begin{aligned}
max(A(\boldsymbol{x})) &\leqslant 35g \\
mean(A(\boldsymbol{x})) &\leqslant 20g
\end{aligned} \tag{5c}
$$

Variables x_6 until x_9 represent the number of layers on zones a, b, c and d in figure 15(b) while variables x_{10} up to x_{13} correspond to the orientation of those layers. The last three variables, x_{14}, x_{15} and x_{16} are core related variables.

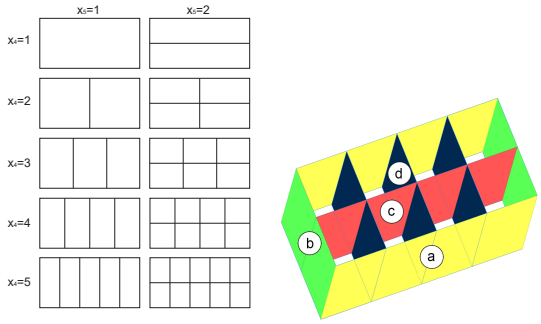

(a) Internal division possibilities.

(b) Carbon Fibre crashbox lay-up scheme.

Figure 15: *Internal division possibilities and lay-up zones.*

In figure 16, all the points that complied with the constraints imposed are represented. The lightest solution has 160.1 grams and reached a maximum acceleration of $165.1 m/s^2$ (solution 2) while the other (solution 1) presented a weight of 288.1 grams and a maximum acceleration of $126.7 m/s^2$.

The only difference between the two non-dominated solutions is the geometry.

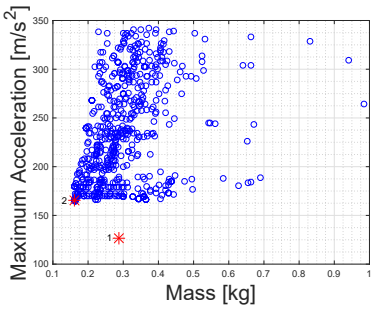

Figure 16: *Nondominated solutions obtained from the Carbon Fibre crashbox optimization.*

It was possible to obtain the optimized geometry and lay-up (figure 17).

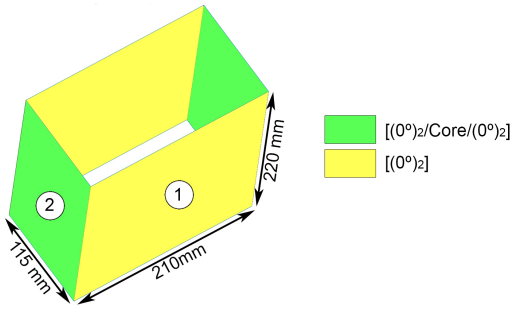

Figure 17: *Geometry and lay-up of the optimized carbon fibre crashbox.*

It was decided that a second, backup option, would be considered where the lay-up from the second wall was also applied on the first wall, ensuring an uniform energy absorption through the cross-section.

A complete assembly analysis must was also made before testing.

The AIP lay-up orientation was defined at $0°$ and the number of layers was iterated until no significant change to the IA behaviour was observed. The AIP lay-up was thus defined as $[(0°)_7/Core/(0°)_7]$.

IV. IA Experimental Results

After weighing three different criteria (solution weight, complexity and material required) the options were organized from best to worst. The three best solutions found were the two CFRP

crashboxes and the alternative design.

i. CFRP Crashbox

The first crashbox to be tested was the optimal result retrieved from the nondominated solutions on section iii.

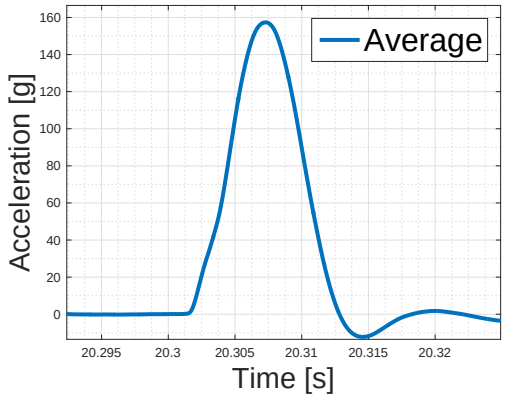

(a) Average performed to the three accelerometers.

Figure 18: *Acceleration results from the first CFRP crashbox tested.*

Data above 40g is present on the raw data so a low-pass filter was applied. In figure 18(a), the average of the accelerometers is performed. However, peaks above the 40g limit are still visible, which means the design has failed.

From the camera's frames, it was possible to calculate the impact duration as 271 frames at 8000 fps meant an impact time of 33.9 ms meaning that the mean acceleration during the impact was 21g, which is higher than the 20g allowed.

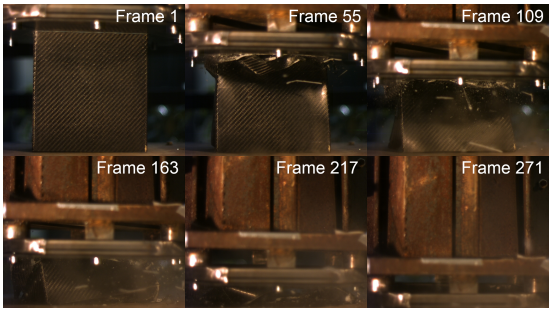

Figure 19: *Frame results from the high-speed camera.*

By looking at the high-speed frames (figure 19) and the debris left by the impact, an explanation to these two failures was proposed.

V. Enhanced Solution

i. CFRP AIP - Numerical Model

After the previous tests, and considering the severe time constraints and resources limitations that formula student teams face, the only viable option left would be to maintain the IA and to design a carbon fibre AIP capable of reducing the overall weight.

A four node orthotropic shell, with a sandwich property, was used to model the AIP.

The AIP lay-up was iterated until no significant difference to the IA behaviour was observed. The lay-up orientation was defined at 0° and a core was assumed to exist only on the red zone in figure 20, in order to reduce the total displacement, while the green centre was reinforced with more layers of carbon fibre to ensure the AIP didn't fail due to the more concentrated loads.

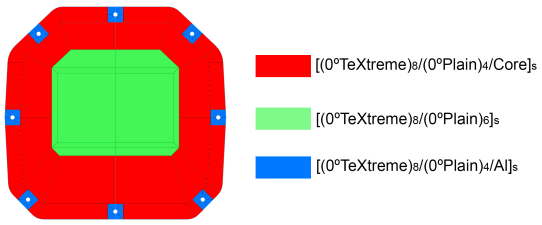

Figure 20: *CFRP AIP.*

In figure 21, the frame results of the impact are presented. Its also observed that the AIP does not fail and that its maximum permanent displacement is rules compliant.

This solution could be further improved by a lay-up optimization process similar to chapter III, this was not done due to the high computational effort required and the tight schedule that the team faced.

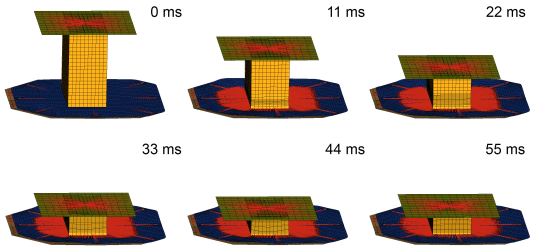

Figure 21: *Frame results of the CFRP AIP with the aluminium honeycomb crashbox.*

ii. CFRP AIP - Experimental Results

Peaks over the 40g limit are present on the raw acceleration data, so a low-pass filter had to be employed, followed by a second order high-pass Butterworth filter (figure 22(a)). As one can see, the maximum acceleration was less than the 40g limit (21.2g) and the average acceleration was also less than 20g (14.6g).

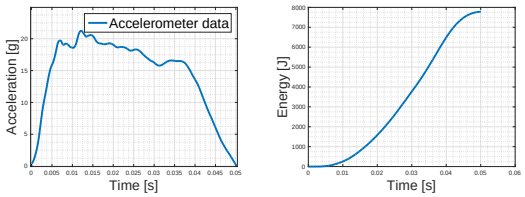

(a) Detail of the first impact. (b) Energy over time.

Figure 22: *Accelerometer data analysis.*

From the acceleration curve, energy plot was computed (figure 22(b)) and it's possible to conclude that the energy absorbed was 7779J, which was higher than required.

According to the rules the AIP maximum permanent deflection is of 25.4mm. In figure 23(a), it's possible to see the AIP and IA assembly before and after the test.

(a) Before the test. (b) After the test.

Figure 23: *Before and after test comparison.*

VI. Conclusions

Preliminary tests were done using aluminium and carbon fibre tubes. Numerical models for both materials were developed and correlated with experimental data. A maximum error of 3.5% and 5% was obtained for the two aluminium tubes tested while, for the carbon fibre tubes, the unknown crush stress parameter was iterated until a fit to the experimental data was achieved. Material characterisation tests were performed on aluminium rods. A simple image tracking algorithm was developed and implemented.

Quasi-static physical tests were developed in order to determine the crush stress property of the laminate used, where a 23.6% lower value was achieved when compared with the experimental data fit. Unaccounted dynamic effects might explain the error obtained.

Based on the carbon fibre numerical model developed, several IA solutions were proposed and analysed. Multiple optimization problems were defined and a very efficient time-saving algorithm was implemented in order to reduce the overall run time to a feasible scale. Even after an optimization process, a coreless structural nose proved to be too heavy (when compared with the current solution). A core was thus allowed to exist and a new optimization process began, effectively reducing the nose weight by 68%. A carbon fibre crashbox was also optimized with respect to its lay-up and geometry which resulted in an IAA weight close to the structural nose (58 grams more).

The IA tests showed flaws in the model regarding the modelling of the core used, namely the single-shell simplification, in impact events. Manufacturing errors related to highly user-dependant processes weren't excluded as they might have caused premature failure.

It was concluded that a single-shell (through thickness) numerical model wasn't able to correctly represent the behaviour observed due to the impossibility for a shell to split into two. Only by adding several shell, or solid, elements through the thickness may this mode of failure be predicted. However, this implies that exten-

sive experimental tests and model tuning needs to be performed in order to extract non-trivial contact properties between the elements.

Nevertheless, a lighter, rules-compliant, solution was proposed, manufactured and tested. By changing the AIP material to a composite sandwich a weight reduction of 500g (22%), when compared with the current solution, was achieved.

References

[1] N. Jones and T. Wierzbicki. *Structural Crashworthiness and Failure*. CRC Press, 1993. ISBN 9781851669691.

[2] a.G Mamalis, M. Robinson, D. Manolakos, G. Demosthenous, M. Ioannidis, and J. Carruthers. Crashworthy capability of composite material structures. *Composite Structures*, 37(2):109–134, 1997. ISSN 02638223. doi: 10.1016/S0263-8223(97)80005-0.

[3] FSAE. FSAE Online. URL `http://www.fsaeonline.com`.

[4] J. Obradovic, S. Boria, and G. Belingardi. Lightweight design and crash analysis of composite frontal impact energy absorbing structures. *Composite Structures*, 94 (2):423–430, 2012. ISSN 02638223. doi: 10.1016/j.compstruct.2011.08.005.

[5] S. Boria and G. Belingardi. Numerical investigation of energy absorbers in composite materials for automotive applications. *International Journal of Crashworthiness*, 17 (4):345–356, 2012. ISSN 1358-8265. doi: 10.1080/13588265.2011.648516.

[6] R. D. Hussein, D. Ruan, G. Lu, and I. Sbarski. Axial crushing behaviour of honeycomb-filled square carbon fibre reinforced plastic (CFRP) tubes. *Composite Structures*, 140:166–179, 2016. ISSN 02638223. doi: 10.1016/j.compstruct.2015.12.064. URL `http://dx.doi.org/10.1016/j.compstruct.2015.12.064`.

[7] S. Heimbs and F. Strobl. Crash Simulation of an F1 Racing Car Front Impact Structure. *7th European LS-DYNA Conference*, (MAY):1–8, 2009. URL `http://www.heimbs-online.de/Heimbs{_}2009{_}Formula1Crash.pdf`.

[8] LS-DYNA. LSTC, 2016.

[9] E. M. Browne. Optimalisert karbonfiber krasjnese for høyytelses Formula Student racerbil. 2016.

[10] a. L. Custódio, J. F. a. Madeira, a. I. F. Vaz, and L. N. Vicente. Direct Multisearch for Multiobjective Optimization. *SIAM Journal on Optimization*, 21:1109–1140, 2011. ISSN 1052-6234. doi: 10.1137/10079731X.

[11] V. M. Franco Correia, J. Madeira, A. Araújo, and C. Mota Soares. Multiobjective design optimization of laminated composite plates with piezoelectric layers. *Composite Structures*, 169:10–20, 2016. ISSN 02638223. doi: 10.1016/j.compstruct.2016.09.052. URL `http://dx.doi.org/10.1016/j.compstruct.2016.09.052`.

[12] K. Miettinem. *Non Linear Multiobjective Optimization*. Kluwer Academic Publishers, New York, 1999.

[13] Abaqus. Dassault Systèmes, 2016.

[14] Tracker. Douglas Brown, 2016.

[15] CZone. Engenuity Ltd., 2016.

[16] A. G. Mamalis, D. E. Manolakos, G. A. Demosthenous, and M. B. Ioannidis. The static and dynamic axial collapse of fibreglass composite automotive frame rails. *Composite Structures*, 34(1):77–90, 1996. ISSN 02638223. doi: 10.1016/0263-8223(95)00134-4.